Mirzaei, Parham A.; Moshfeghi, Mohammad; Motamedi, Hamid; Sheikhnejad, Yahya; Bordbar, Hadi

A simplified tempo-spatial model to predict airborne pathogen release risk in enclosed spaces: An Eulerian-Lagrangian CFD approach

Published in:
Building and Environment

DOI:
10.1016/j.buildenv.2021.108428

Published: 01/01/2022

Document Version
Peer-reviewed accepted author manuscript, also known as Final accepted manuscript or Post-print

Cite the paper as : Mirzaei P., Sheikhinejad Y., Moshfeghi M., Motamedi H., Bordbar H., (2022), "A simplified CFD-based demographical model for COVID19 virus-laden respiratory aerosol release: an artificial intelligence based statistical-Eulerian-Lagrangian CFD approach", *Building and Environment, Vol. 207,* pp. 108428, https://doi.org/10.1016/j.buildenv.2021.108428.

A Simplified Tempo-spatial Model to Predict Airborne Pathogen Release Risk in Enclosed Spaces: an Eulerian-Lagrangian CFD Approach

P A Mirzaei[1*], M Moshfeghi[2], H Motamedi[3], Y Sheikhnejad[4,5], H Bordbar[6]

[1] Architecture & Built Environment Department, University of Nottingham, University Park, Nottingham, UK

[2]Department of Mechanical Engineering, Sogang University, Seoul, Korea

[3]Department of Mechanical Engineering, Tarbiat Modares University, Iran

[4]Centre for Mechanical Technology and Automation, Department of Mechanical Engineering, Universidade de Aveiro, 3810-193 Aveiro, Portugal

[5]PICadvanced SA, Creative Science Park, Via do Conhecimento, Ed. Central, 3830-352 Ílhavo, Portugal.

[6]School of Engineering, Aalto University, Finland

[*]Corresponding author: Parham.Mirzaei_Ahranjani@nottingham.ac.uk

Abstract

COVID19 pathogens are primarily transmitted via airborne respiratory droplets expelled from infected bio-sources. However, there is a lack of simplified accurate source models that can represent the airborne release to be utilized in the safe-social distancing measures and ventilation design of buildings.

Although computational fluid dynamics (CFD) can provide accurate models of airborne disease transmissions, they are computationally expensive. Thus, this study proposes an innovative framework that benefits from a series of relatively accurate CFD simulations to first generate a dataset of respiratory events and then develop a simplified source model.

The dataset has been generated based on key clinical parameters (i.e., the velocity of droplet release) and environmental factors (i.e., room temperature and relative humidity) in the droplet release modes. An Eulerian CFD model is first validated against experimental data and is then interlinked with a Lagrangian CFD model to simulate trajectory and evaporation of numerous droplets in various sizes (0.1 μm to 700 μm). A risk assessment model previously developed by the authors is then applied to the simulation cases to identify the horizontal and vertical spread

lengths (risk cloud) of viruses in each case within an exposure time. Eventually, an artificial neural network-based model is fitted to the spread lengths to develop the simplified predictive source model. The results identify three main regimes of risk clouds, which can be fairly predicted by the ANN model.

Keywords: Tempo-spatial Risk Model, COVID19, airborne pathogen transmission, Eulerian-Lagrangian-CFD, respiratory disease, artificial neural network

1. Introduction

The primary transmission mode of COVID19, as a rapidly spreading airborne disease, is understood to be in-person exposure to infected people's respiratory secretions and bioaerosols expelled in various sizes (1). Before reaching an effective vaccine, social distancing remains the inevitable defensive measure during pandemics. Maintaining a physical distance between people, as one of the means of social distancing, is enforced by many governments worldwide, while the essence of such stipulated measures is adapted from early evidence regarding the release and environmental persistence of SARS-CoV2 (2).

From fluid dynamics perspectives, COVID19 transmission mode via respiratory bioaerosols requires a thorough investigation of droplets' number, size, and density distribution as well as their initial velocities (3). It is widely agreed that heavy droplets will deposit within less than a meter (4), while micron-size airborne droplets could travel to a much longer distance following the air stream (5). Nonetheless, the effectiveness of such physical distance policies is controversial on many occasions as the bioaerosol release mechanisms from respiration, sneeze, and coughs are chronically underestimated in past studies.

***Table 1**. List of effective factors in bioaerosol release*

#	Item [unit]	Reported Interval	Reference
1	Bioaerosol size distribution [μm]	0.5 – 2,000	(4, 6)
2	Number of bioaerosol/particles	5,000, 9×10^6	(6, 7)
3	Environment property	Walls, windows, partitions, etc.	
4	Local ambient air velocity[m/s]	[0.25-1.5], 21.7, 0- 10	(7, 8)
5	Local ambient air direction [deg]		(9)
6	Local ambient air humidity [%]	[20 – 60], 50	(6, 8)
7	Local air temperature [^oC]	[17-23], 25,	(7, 8)
8	Temporal profile of exhalation flow rate (for C or S) [m^3/s]	Fig. 5(a)	(8, 10, 11)
9	Spatial profile of exhalation [-]		(12, 13)
10	With or without facial mask	[with or without]	(11)
11	Gender [-]	Man, Woman	(14)
12	Age [year]	19 - 50	(15)

The place of disagreement in contradictory findings associated with the disease transmission are in numerous strands, including carriage process of pathogens with droplets and aerosols from an

infected person to a new host (16), drying and evaporation processes of exhaled bioaerosols following with its properties (e.g., size, mucus), environmental conditions (e.g., relative humidity) (6, 17), and number and size of released bioaerosols in each activity mode (i.e., respiration, sneeze, and coughs) (8, 18, 19). As it has been broadly discussed in previous studies, one should add the importance of demographical characteristics (age, gender, ethnicity, etc.) on the bioaerosol release mode. Some of these understandings are summarized as 12 pivotal factors in **Table 1**. These are the effective parameters that may influence bioaerosol release and dispersion. Many of these parameters ultimately alter the volume and speed of respiratory droplets release and therefore can be represented by the velocity of two-phase respiratory flow at the mouth. Hence, in this study, the effective parameters are shortlisted to three major ones to lower the computational costs and carry out the calculations in a practical timeline.

The identified parameters in **Table 1** are supported by careful experimental and observational studies from various methodological perspectives, including medicine, statistics, fluid dynamics, etc. For example, the National Institute for Occupational Safety and Health (20) constructed a cough aerosol simulator that produces a humanlike cough in a controlled environment based on coughs recorded from influenza patients. The total aerosol volume expelled during each cough was monitored to be 68 μL using aerosol generated from a cell culture medium. As another PIV study to measure coughing velocity, Kwon et al. (12) obtained the average initial coughing velocity of 15.3 m/s for males and 10.6 m/s for females while the average initial speaking velocity was measured around 4.07 m/s and 2.31 m/s, respectively; the angle of the exhaled air from coughing was reported around 38° for the males and 32° for the females while that of the exhaled air from speaking was around 49° and 78°, respectively. In another conditioned indoor environment, Zhang et al. (8) reported the distribution of generated aerosol from a horizontal coughing mode using a manikin in the presence of 16 diffusers mounted on walls. In another study, an experimental cough aerosol detection via laser diffraction system from 45 healthy people presented a demographic statistical analysis of bioaerosol size by sex and age (15).

Respiration, speech, sneeze, and cough (RSSC) flows carry bioaerosols, the size of which significantly varies through the particles' path line. Larger droplets (>50-100 μm) are mainly governed by gravity. The intermediate (10-100μm) and small (<5-10 μm) droplets are more affected by airflow and ventilation streams and may travel much further. At the same time, the evaporation process changes the intermediate size droplets of RSSC to become airborne and stay floating in the air, which particularly highlights the role of ventilation and air humidity. For instance, the drying times for 50μm and 100μm droplets at a 50% relative humidity are reported

to be 0.3 and 1.3s, respectively (36). Even after complete evaporation, the small dried aerosol particles can potentially carry viruses as the usual size of viral pathogens is 25 nm to 5 μm (5). For small droplets with a low Stokes number ($St \ll 1$), the sedimentation time is longer than the time needed for a complete evaporation process, and the small droplets become airborne. Therefore, they turn suspended in the air and move with the air stream, increasing the risk of virus transmission to a much longer distance. A schematic description of bioaerosols behaviour is shown in **Figure 1**.

Yet, the role of airflow transport as the delivery route of pathogens in smaller size droplets (< 50 μm) is not well investigated, while larger size droplets (> 50 μm) are commonly accepted to follow ballistic trajectories being mainly governed by gravity. More recently, lingering small size airborne droplets (<5 μm) is suggested to be another plausible root in airborne disease transmission (21). Although advanced methods, including particle image velocimetry (22, 23), and laser diffraction system (15), to trace particles have been around in-hand for years, these approaches were barely successful in extending the knowledge in tracing airborne disease transmission in buildings and the built environment. Due to the high expenses, time constraint of set up, and limitation of devices in monitoring smaller scale droplets, experimental studies only cover a limited spectrum of droplet size, number, injection velocities released from sources (i.e., the mouth of people). The movement of occupants in the room, due to its impact on airflow patterns inside the enclosed areas, was also a subject of several studies. Shih et al. (24) numerically investigated the impact of person movement and door opening and closing on flow distribution inside a hospital isolated room. They found that both movement and door sliding have temporal impacts on the flow distribution inside the room. In another study, Wang et al. (25) employed CFD to investigate the impact of walking on the dispersion of exhaled droplets in an isolated room. Their simulation results showed that the local environment around the person could be affected by walking. They also reported that increasing the walking speed decreases the concentration of suspended airborne particles.

Computational Fluid Dynamics (CFD) is, therefore, a cheaper alternative, widely used to overcome the shortcomings of experimental and observational studies. In this respect, high-fidelity CFD models validated against observational datasets have been developed on Lagrangian perspectives as flexible tools to further investigate the parameters impacting the release and spreading of bioaerosols (5), particularly the transport process of smaller scale droplets. Some of the numerical studies addressed the human respiration process and the transport of exhaled air by breathing, sneezing, and coughing, and their potential impact on the adjacent person (26), (25), (27), (28). Discrete and continuous models of droplets in multiphase turbulent buoyant

clouds are studied by (29) with suspended droplets of various sizes. These studies highlighted that cough and sneeze airflows are multiphase turbulent buoyant clouds with suspended droplets of various sizes. The droplets can remain suspended in the cloud until their settling speed matches that of the decelerating cloud. In addition, the 3D transient CFD model is used by (30) to predict personal exposure times to airborne pathogens and thus the infection risk in a displacement ventilated room. Authors showed that for short separation distances, the interaction between breaths is a key factor in the airborne cross-infection. Li et al. (31) studied the evaporation and dispersion of cough droplets by Lagrangian-Eulerian model in quiescent air, considering inhomogeneous humidity field, and demonstrated that evaporation-generated vapor and super-saturated wet air exhaled from the respiratory tracks forms a vapor plume in front of the respiratory tract opening. Interestingly, due to the droplet size reduction induced by evaporation, both the number density of airborne droplets and mass concentration of inhalable pathogens remarkably increased, which may increase the risk of infection. Moreover, the physics of aerosol and droplet dispersion and distribution of droplet aerosols were investigated from mouth coughing and nose breathing using LES by (5) and (8). It is reported that the typical size range of speech and cough originated droplets (d 20 μm) can linger in the air for hours so that they could be inhaled and rapid drying process of even large droplets, up to sizes O(100 μm), into droplet nuclei/aerosols was observed. Another critical parameter in the time-dependent dispersion of cough droplets, namely the effect of the human body by a 3D thermal manikin was, investigated by (32) while due to the buoyancy-driven thermal flow, both the vertical velocity and displacement of small droplets (≤20 μm) were completely reversed from descending to ascending. Also, another recent experimental and numerical study on the transport of droplet aerosols in a fever clinic showed that the best ventilation performance appeared for a patient sitting and coughing while the case of a patient lying and talking was the worst case (31). In another clinical experiment, the size of droplets were measured in an indoor environment, with an air temperature of 18 ^{o}C and relative humidity of 50%, the horizontal range of large respiratory droplets (diameter 120 μm–200 μm) in speaking were between 0.16 m to 0.68 m, in coughing, between 0.58 m to 1.09 m, and in sneezing between 1.34 m to 2.76 m. (32). Also, results from comparative studies on transport characteristics of contamination dispersion in a passengers' local environments revealed significant increases of residence times (up to 50%) and extended travel distances of contaminants up to 200 μm after considering cough flow, whereas contaminants travel displacements still remained similar (33).

Despite the necessity to employ Lagrangian CFD models to trace the small particles, as explained above, such models demand intensive computational resources, which hinder a comprehensive

investigation of the bioaerosol release process regarding its various affecting parameters. This implies that Lagrangian simulations are costly choices to be directly applied to represent humans as the source of bioaerosol release in many practical scenarios where multiple occupants interact in mechanically or naturally ventilated environments. Nonetheless, developing a reliable bioaerosol release source is vital for the design and control of ventilation design, space management, and social distancing, especially during pandemics. Hence, similar to many other simplified source term models of a human body such as the amount of heat or CO_2 releases widely used in buildings' design and control applications, a simplified airborne pathogen droplet release model is necessary to be applied as a source term to other models.

To address this shortcoming in providing a deep insight related to virus-laden bioaerosol release from human sources in indoor and outdoor spaces, this study proposes a framework to develop a simplified model of droplets' release from respiratory events (here sneeze and cough). This model encompasses a range of droplet release modes related to clinical (i.e., droplet release velocity from the bio-source mouth) and environmental (i.e., room temperature and relative humidity) distribution of bio-sources using an Eulerian-Lagrangian CFD model. The effective parameters on droplet release from bio-sources are initially synthesized to define a series of airborne pathogen release scenarios (35 cases). These scenarios are then simulated with a series of computationally intensive Eulerian-Lagrangian CFD simulations to construct a repository dataset. The dataset is then fed into a risk assessment model (RAM) previously developed by authors (35) to account for the tempo-spatial risk analysis of the respiratory event rather than the instantaneous release of droplets. In a later step, the tempo-spatial risk data is fitted to an artificial neural network model capable of predicting the risk cloud expansion of a bio-source throughout time. It should be noted that the background airflow of the studied enclosed space is assumed as still air condition, so that the initial behavior of droplets' transport can be observed. The human source is considered to have a fixed position in the room, and its movements are not taken into account in this study. Nonetheless, the proposed framework demonstrates the flexibility to add any complex background airflow that may be caused by bio-source movement, ventilation systems, etc.

In addition, to develop artificial intelligence (AI) to predict numerical results of CFD simulation, the powerful branch of AI, namely multi perceptron feedforward version of artificial neural network, is adopted with deep learning to generate an accurate prediction for unseen conditions. Its code is developed in Python program language, and the number of neurons, as well as other settings such as learning rate, are tuned, and tailored for this specific work.

Regarding the structure of this paper, Section 2 describes the methods used to develop the Eulerian-Lagrangian CFD model risk assessment model. It also briefly explains the risk assessment model. Section 3 presents the scenarios designed to cover a range of airborne pathogen release modes. Finally, Section 4 provides the results, followed by the discussions and conclusion sections.

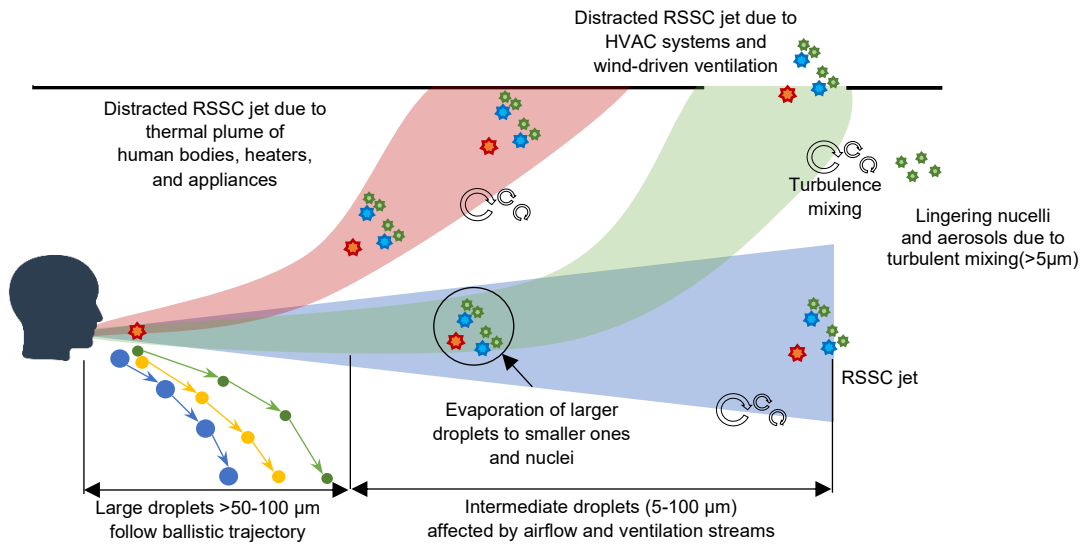

***Figure 1**. Airborne pathogen respiratory droplet release mechanism in an enclosed environment*

2. Method

2.1. Proposed Framework of Airborne Pathogen Respiratory Aerosol Release Model

As stated before, comprehensive Eulerian and Lagrangian CFD modeling of airborne pathogen respiratory aerosol release takes intensive computational cost even after using high-performance and cluster computing resources. Furthermore, as addressed in **Table 1,** the bioaerosol release has been found to depend on several parameters. Thus, reaching a comprehensive model, undertaking airborne pathogen respiratory droplets release rate of any individual, is an impractical approach, following the existing methods in the literature. Hence, this study proposes an innovative approach to substantially decrease the computational burdens while underpinning the necessary complexities of such phenomena. The proposed framework benefits from different tools to systematically develop a simplified model to be used for ventilation design or social distancing control in spaces.

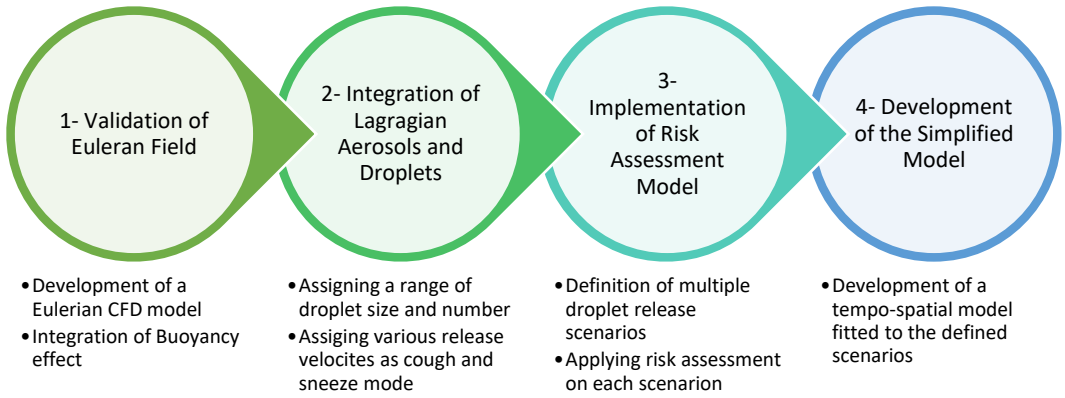

***Figure 2**. The framework of simplified CFD-based demographical model for COVID19 virus-laden respiratory aerosol release*

For this purpose, as depicted in the framework of **Figure 2**, four steps are considered to generate the simplified bio-source model. In Step-1, an Eulerian CFD model is first developed to accurately replicate the flow field in a room with a still background airflow field. While the buoyancy effect due to the room temperature stratification and jet release temperature is taken into account, the flow streams are successfully validated with an experimental study by (39).

Step (2) is dedicated to accurately modeling large to small droplet movements via a Lagrangian CFD model, which is then coupled with the Eulerian model to reproduce the velocity field at an acceptable level while fast due to its low and yet precise enough number of cells. At this stage, parameters of **Table 1** have been analyzed and shortlisted to the three most important ones (i.e.,

bio-source velocity, room temperature, and room RH). Thirty-five scenarios have been generated to cover a wide range of rooms' conditions and bio-source release velocities related to sneeze and cough modes. It should be noted that due to the extensive computational cost of a potential high-resolution CFD model, a comprehensive study is firstly conducted to find a model with a coarser mesh size, which can simultaneously provide a fair level of accurate results.

Within Step-3, a risk assessment model previously developed by authors (34) is implemented to translate the CFD simulations to a time series of airborne pathogen disease transmission risk in the vicinity of the bio-source. The RAM model, thus, provides the tempo-spatial risk of infection in the studied room. This implies that the maximum horizontal and vertical distances from the infected bio-source with a considerable level of risk calculated by RAM are assumed as the risk cloud of that case study.

Eventually, in Step-4, the calculated maximum distances (risk clouds) of all case studies generated in the previous step are used to train a simplified model using the artificial neural network (ANN) technique. In this model, the release velocity, room temperature, and RH are the inputs, and the tempo-spatial risk cloud is the output.

2.2. Eulerian CFD Model

An Eulerian method is applied to model the unsteady incompressible flow field using Navier-Stokes as the governing equations for mass, momentum, and energy equations:

$$\frac{\partial U_i}{\partial x_i} = 0 \tag{1}$$

$$\frac{\partial U_i}{\partial t} + \frac{\partial (U_j U_i)}{\partial x_j} = -\frac{1}{\rho}\frac{\partial P}{\partial x_i} + \frac{\partial}{\partial x_j}\left(\vartheta \frac{\partial U_i}{\partial x_j} - \overline{u_i' u_j'}\right) \tag{2}$$

$$\frac{\partial T}{\partial t} + \frac{\partial (U_j T)}{\partial x_j} = \frac{1}{\rho C_p}\frac{\partial}{\partial x_j}\left(k\frac{\partial T}{\partial x_j} + \left(\vartheta \frac{\partial U_i}{\partial x_j} - \overline{u_i' u_j'}\right) U_i\right) \tag{3}$$

where $\overline{u_i' u_j'}$ is the Reynolds stress tensor, which is modeled by the Boussinesq hypothesis. SST k-ω is also used as the turbulence model (40).

2.3. Lagrangian Discrete Phase Model

Particles are modeled based on a Lagrangian-Eulerian approach using SimcenterSTAR-CCM+Ver. 13.06.12 (double precision), where the conservation equations of mass, momentum,

and energy for the dispersed phase are derived for each particle in a Lagrangian form to calculate their trajectories.

2.3.1. Equations of Motion for Particles

As a general method for particle, droplet, and bubble, the trajectories of discrete phases (i.e., respiratory droplets) are resolved by integrating a force conservation equation on each particle, written in a Lagrangian reference frame:

$$\frac{du_p}{dt} = F_D(u - u_p) + g_i \frac{(\rho_p - \rho)}{\rho_p} + F_i \quad (4)$$

where "*i*" is the coordinate direction (*i* =x,y, or z), and subscript "p" represents particles. u and ρ are the fluid phase velocity and density, respectively. F_i is the force per unit particle mass (acceleration), and the term $F_D(u - u_p)$represents an additional acceleration (force per unit particle mass) in which F_D is calculated as:

$$F_D = \frac{18\mu}{\rho_p d_p^2} \frac{C_D\, Re}{24} \quad (5)$$

whereμ is the molecular viscosity of the fluid, and d_p is the particle diameter. Also, Re is the relative Reynolds number, which is calculated as:

$$Re = \rho(u - u_p)d_p/\mu \quad (6)$$

Since the dispersed droplets are volatile, the mass transfer occurs between the phases accompanied by an interphase heat transfer. Hence, heat transfer occurs because of the interphase temperature differences, and the interphase mass transfer changes the sizes of the droplets as described in the following sub-sections.

2.3.2. Particle Mass Balance

The equation related to the conservation of mass of a particle can be expressed as:

$$\frac{dm_p}{dt} = \dot{m}_p \quad (7)$$

where m_p denotes the mass of the particle, and $\dot{m}_p$ represents the rate of mass transfer to the particle. The latter is a non-zero value for the simulations, which include the evaporation process.

2.3.3. Droplet Evaporation

The multi-component droplet evaporation model used in this study assumes droplets to be internally homogeneous, consisting of an ideal mixture of liquid components subject to vaporization. Moreover, the model assumes inert components in both the droplet and the gas. Regarding the evaporation of multi-component droplets, $\dot{m}_{pi}$ is defined as the rate of change of mass of each transferred component due to quasi-steady evaporation:

$$\dot{m}_{pi} = -\varepsilon_i g^* A_s ln\,(1 + B) \tag{8}$$

where g^* represents the mass transfer conductance, and B is known as the Spalding transfer number. Also, "*i*" is the index of each component in the mixture, and ε_i represents the fractional mass transfer rate for which the sum of all *N* components complies with the following equation:

$$\sum_{i=1..N} \varepsilon_i = 1.0 \tag{9}$$

2.3.4. Particle Energy Balance

As a basic assumption for material particles, one can assume that particles are internally homogeneous. From a thermal point of view, this is equal to a low Biot number (<0.1). The equation of conservation of energy will be:

$$m_p c_p \frac{dT_p}{dt} = Q_t + Q_{rad} + Q_s \tag{10}$$

where Q_t is the rate of convective heat transfer to the droplets from the continuous phase, Q_{rad} represents the rate of radiative heat transfer, and Q_s is related to other heat sources.

2.4. CFD Domain, Mesh, and Boundary Conditions

The computational domain has a size of 3.5m × 3.5m × 6m, as shown in **Figure 3Error! Reference source not found.**, representing a room without ventilation. Droplets with different diameters from 0.1μm to 700μm, caused by the exhalation, were released from a circular area with a diameter of 1.2 cm located at the center of a 3.5m × 3.5m wall (30). It is worth noting that the mouth diameter (1.2 cm) has been chosen slightly smaller than the value of 1.5 cm that was used by Chao et al. (44) for the average mouth diameter of eight university students (under 30 years old). While these two values are in the same range, the smaller mouth diameter in the present research assumes the respiratory event might be released by patients of younger ages or smaller body sizes.

The dimensions of this domain have been selected after a series of preliminary simulations, ensuring the adequacy of the room dimensions for analysis of airborne behavior of the droplets where the exhalation jet reaches a velocity value in the order of 2cm/s (less than 1% of the jet velocity) before it reaches the wall in the front of the side of the mouth (located at x=6m) (41). The results implied that after simulating an adequate physical time, droplets with the diameter of 10μm or below linger in a range up to 6m from the releasing surface with a velocity below 2cm/s while droplets with the diameter of 100μm are deposited in smaller distances of about 1m from the jet inlet.

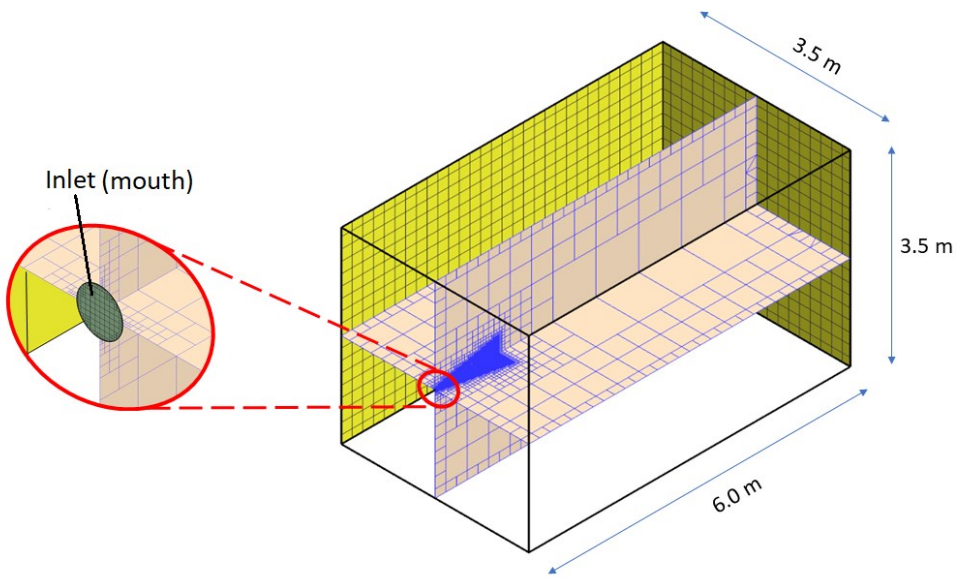

***Figure 3**. Mesh distribution around the jet centerline*

To ensure the final size of the utilized mesh in a reasonable time frame, different grid resolutions with hexahedral cells were tested, ranging from 189k cells to 4.5M cells. The optimal mesh was identified as the 189k-HYB case, which has minimum and maximum cell sizes of 0.06m and 0.2m, respectively, with a surface growth rate of 2.0. It should be noted that a conic volume with a length of 1 m dense cells was generated around the mouth of the bio-source, as seen in **Error! Reference source not found.**. All surfaces were considered as solid walls with no-slip boundary conditions (see Table 2). Wall treatment is based on an adaptive approach. The other boundary conditions of the model are presented in **Error! Reference source not found.**.

Proper simulation of exhalation activity requires reliable data on the size distribution of droplets and transient exhaled airflow profile. **Error! Reference source not found.** presents air velocity profiles and droplet size distributions of sneeze and cough, resulting from massive measurements on people of different ages and gender.

***Table 2**. Droplet and background air properties*

Droplet properties	**Mass fraction [%]**	**Density [kg/m^3]**	**Specific heat capacity [J/Kg-K]**	**Saturation pressure [Pa]**
Non-evaporative	3 (42)	1280.8	2404.6	
Evaporative	97 (42)	997. 6	4181.7	3170.3
Air Properties	**Dynamic viscosity [Pa-s]**	**Molecular weight [Kg/Kmol]**	**Specific heat capacity [J/Kg-K]**	
	1.855×10^{-5}	28.97	1003.6	
Droplet size and number	Profiles in **Error! Reference source not found.**Error! Reference source not found.			

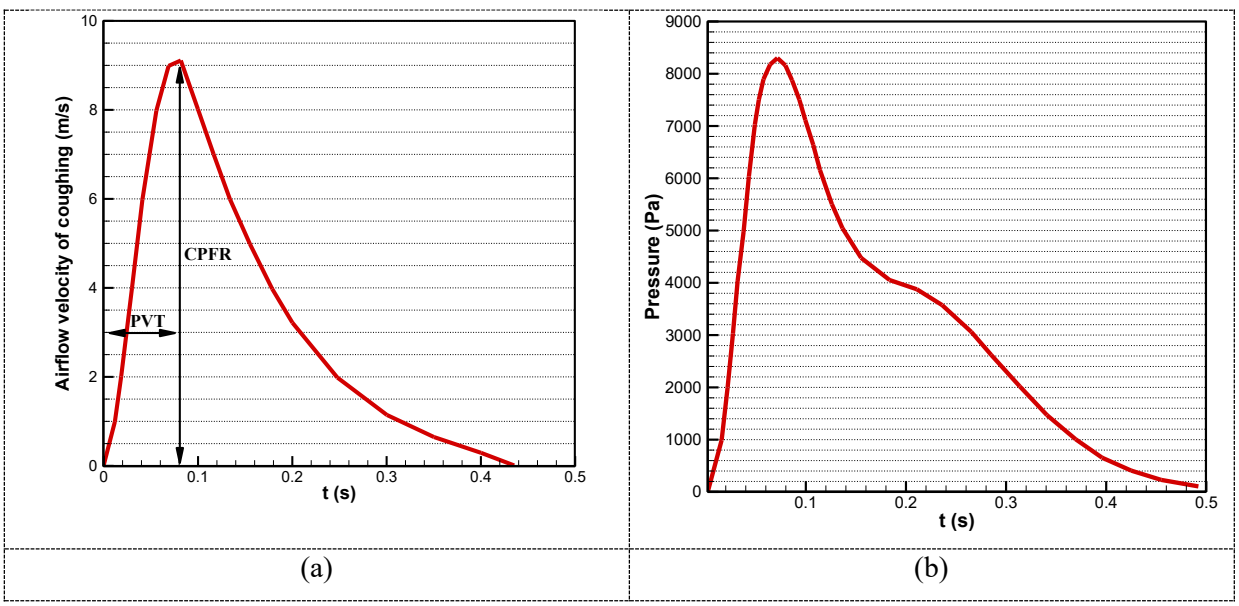

(a) (b)

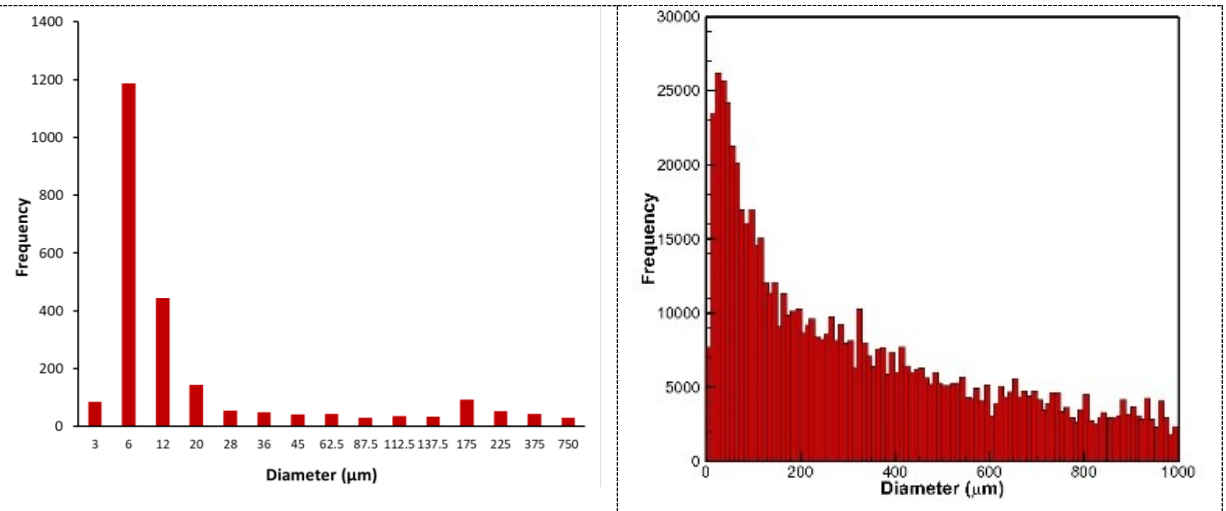

(c)	(d)

Error! Reference source not found.. Extracted velocity profile of (a) cough (8), and (b) sneeze (43) and droplet size histogram of (c) cough (44), and (d) sneeze (45)

2.5. CFD Setting

In the present transient CFD simulations, the background air was simulated as a non-reactive ideal gas composed of standard air and some amount of water vapor, depending on the relative humidity of each case (see Table 2). The results of the simulations, conducted within 60 seconds, implied that the droplets with a diameter of 10 μm or below had become airborne, traveling not more than 5 m from the mouth, while droplets with a diameter of 100 μm fell at short distances of about 1 m from the jet inlet.

The droplets were simulated as discrete phases using the Lagrangian model and were assumed to have spherical shapes. To mimic realistic pathogenic droplets, they were assumed to be initially composed of 3% non-evaporative and 97% evaporative mass fractions. The density of the non-volatile fraction was 1280.8 $kg.m^{-3}$ with a specific heat transfer of 2404.6 $J.Kg^{-1}.K^{-1}$ at the standard state temperature of 298.15 K. On the contrary, the evaporative portion was assumed as water with a density of 997.6 $kg.m^{-3}$ and a specific heat transfer of 4181.7 $J.Kg^{-1}.K^{-1}$ at the same standard state temperature. In addition, the saturation pressure of this evaporative fraction (water) was set to 3170.3 Pa. The mass-weighted mixture was used for the calculation of the density and specific heat of each droplet. For each droplet's outer surface, it was assumed that the droplets would stick to any wall surface of the room as they reached them. As an averaged value, periodicity of cough and sneeze were considered 0.6 second. At each simulation, cough

or sneeze were modelled by a normal breathing velocity of about 1 m/s and intermittence of 5 times a minute.

Similar to the Lagrangian model, the weighted mixture method for the Eulerian model was employed for the calculation of the air-water mixture in the background air. Finally, the aerodynamic interaction between the particles and the air has been simulated using drag force calculated by Schiller–Naumann's drag force coefficients and the pressure gradient force.

The turbulence is modelled using Realizable k-epsilon model with “All y+ wall treatment” option in STARCCM, making the model suitable for the coarse and fine meshes. In should be noted that the Realizable k-epsilon is classified under High Reynolds Number turbulence models, and its Y+ can be 100 or even higher. In the present simulations, the Y+ was about 10, which is out of the critical range [11.04~30]. In addition, the "two-layer, all Y+ wall treatment" option in STARCCM adjusts the wall functions for any Y+ in areas near the mouth with smaller Y+ [40]. It is also worth mentioning that since the present does not work with any flow details near the walls and flow velocity near the walls was almost zero, we believe that the expansion ratio equal to 2 would be a good choice and does not affect the accuracy of problem for the still flow as the air velocity is zero.

The discretization scheme is a second-order one for momentum equations. The energy equation is activated to include the evaporation of the droplets. All simulations proceeded as transient simulations with a timestep of 0.01 second and 20 inner iterations. Due to the high computational cost of the transient solution, the level of convergence was set not smaller than10^{-4}. Yet, each case was taken about 16 hours for a typical simulation time for 60 [s] using the computer cluster at Sogang University with 24 computational cores with Xeon(R) 2.20GHz CPUs.

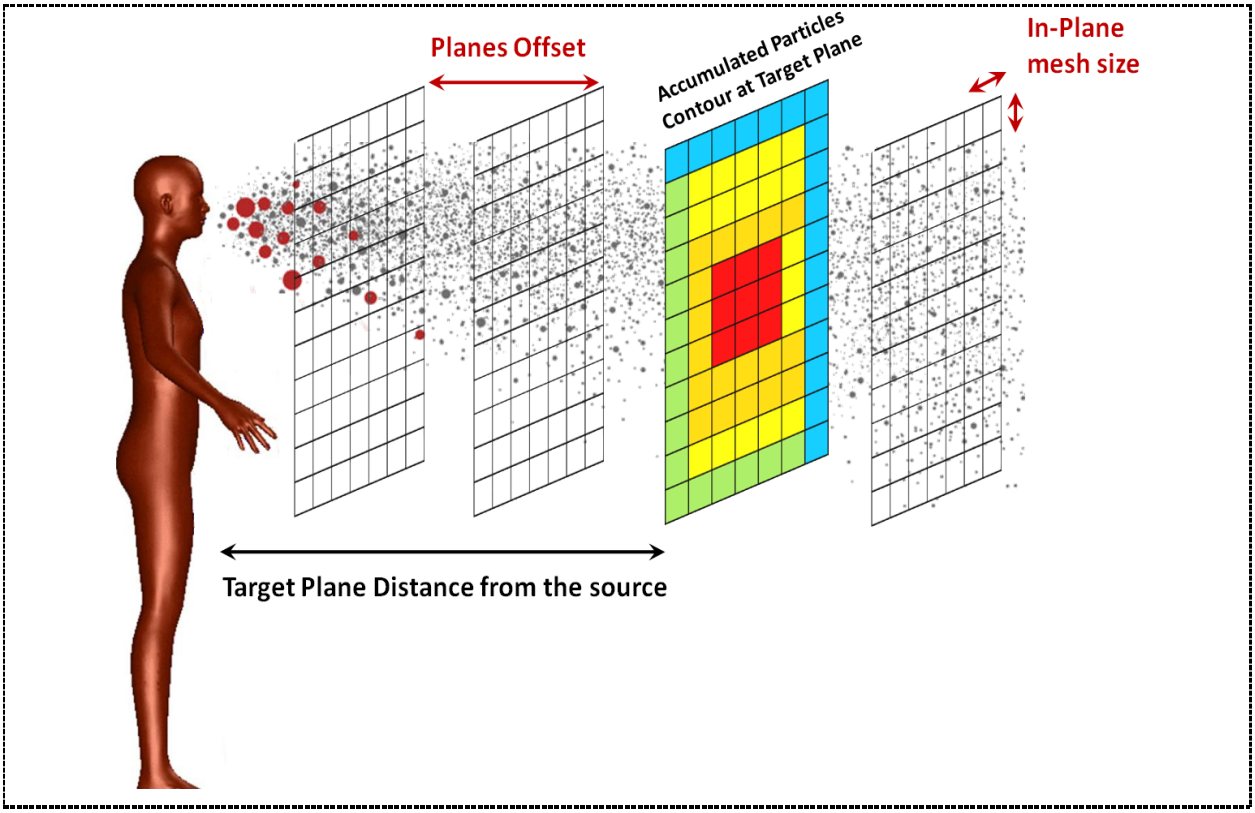

Figure 4*.The secondary mesh and pathogen droplets passing through the vertical planes' cells*

2.6. Risk Assessment Model

When performing Lagrangian simulations, CFD solvers normally report instantaneous data of droplets such as position, velocity, and diameter. While the infection risk at each position of the room is associated with the accumulated number of droplets passing from that point within a specific time interval. On the other hand, medical science suggests that a disease transmission with airborne pathogens happens when a person inhales a certain dosage of infected droplets.

A previously developed risk assessment model (RAM) by authors thus calculates the accumulated droplet passing at each space location. For this purpose, RAM generates a uniform coarse mesh inside the domain, known as secondary mesh (shown in **Figure 4**), and according to available output data of droplets generated by the CFD solver at each time-step, it predicts the position of droplets at previous time-steps and consequently computes the accumulated number of particles at each cell of the secondary mesh within the time-span of the simulation. RAM includes multiple steps to count the number of droplets with different droplet sizes from sub-micron to hundreds-micron released from respiratory jet and passing through a specific location of an enclosed space. Therefore, this leads to a 3D temporal profile, which shows a temporal risk

cloud being expanded around a bio-source. Details of RAM developed by authors and applied algorithm can be found in (34).

2.7. Artificial Neural Network

A deep ANN with feed-forward multi-layer perceptron architecture has been used in this study (46). A back-propagation learning paradigm was employed to build the surrogate model. The continuous nonlinear sigmoid function with smooth gradient was employed in the model due to its proven capability in making clear distinctions on predictions. A comparison was conducted among five different architecture of ANN in terms of hidden layers and number of neurons to find the best architecture that delivers the best predictive results. The analysis was performed under the circumstances that the ANN was fully unsighted on all 60 values (secondly-basis CFD data for one minute) within each two test cases. As shown in **Table 3**, the 10×10 ANN was eventually selected due to showing the least averaged testing error among other architectures. More hidden layers can potentially result in overfitting due to the nature and size of the data.

***Table 3**. The averaged ANN training and testing error after 20,000 iterations*

NN Architecture	Averaged ANN training error	Averaged ANN testing error
5×5 ANN	13.3%	34.2%
9×9 ANN	11.5%	31.6%
10×10 ANN	9.25 %	29.6%
20×20 ANN	10.12%	32.1%
30×30 ANN	12.9%	33.7%

3. Case Study

3.1. Airborne Pathogen Release Scenarios

Eulerian-Lagrangian CFD simulations are computationally cumbersome tasks to be conducted for many scenarios related to various airborne pathogen droplet releases from human sources. However, by implementing the design of experiment (DoE) technique, the intensive computational burden related to the number of needed simulations is substantially reduced. For this purpose, 12 parameters (e.g., droplet size, number of droplets, the temporal, and spatial profile of cough) are initially identified as the effective parameters (see **Table 1**). After scrutinizing a comprehensive literature review and implementing further assumptions when data does not exist, three parameters, including droplet release velocity from bio-sources, room temperature, and room's relative humidity, are utilized as the effective parameters while considering a minimum of three levels for each parameter. Each parameter is then varied with three increments to initially populate

27 cases, as presented in Table 4. After analyzing the data as presented in the results section, eight additional cases were added to improve the training of the ANN model. As mentioned in Section 2.6, each case has an array of 60 values on a secondly-basis that shows the evolution of vertical spread over 60 s. Furthermore, two cases were used only to validate the model and were not included in the training steps. Although considering 35 cases is not ideal for three main identified parameters, the ANN results shown in the following sections reveal the capability of the model to capture a relatively correct vertical and horizontal spread, which satisfies the main aim of this study to develop a simplified model in recognizing such distances.

Table 4. *Respiratory cough and sneeze simulation scenarios*

	Case ID	**Max. Velocity (m/s)**	**Room Temp. (℃)**	**Room RH (%)**
Main cases	1, 2, 3	18	15	20, 50, 80
	4, 5, 6		22	20, 50, 80
	7, 8, 9		29	20, 50, 80
	10, 11, 12	34	15	20, 50, 80
	13, 14, 15		22	20, 50, 80
	16, 17,18		29	20, 50, 80
	19, 20, 21	50	15	20, 50, 80
	22, 23, 24		22	20, 50, 80
	25, 26, 27		29	20, 50, 80
	Case ID	**Max. Velocity (m/s)**	**Room Temp. (℃)**	**Room RH (%)**
Additional cases	**28**	34	29	60
	29	34	15	10
	30	25	25	65
	31	18	18.5	50
	32	34	29	70
	33	34	29	75
	34	25	15	50
	35	25	15	20
Validation (test) cases	**T1**	50	22	80
	T2	34	18.5	50

4. Results and Discussion

4.1. Mesh Sensitivity Analysis

Since the most crucial parameter for particle dispersion is air velocity, before the main simulations, a mesh sensitivity analysis has been performed to ensure that the final mesh and the velocity field are independent of the element size. For this part, the flow velocity in the far-field zone (i.e., the distance where $y/d_0 > 20$ from the mouth) was investigated, and the results were later validated against the experimental by [39]. The inlet velocity had spanwise (along with discharge hole radii) as well as streamwise (centreline) velocity profiles with the maximum value of 20 m/s. For this purpose, four meshes with different resolutions with hexahedral cells were generated, containing a total mesh number of 189k, 627k, 3.7M, and 4.5M.

After this preliminary study, it was observed that a minimum number of 3.7M cells was required for an independent mesh resolution. However, since this research needed a large number of simulations and this could result in an unaffordable computational cost, and also aligned with the aim of this study to develop a simplified model, the viable solution was to generate a mesh, which is relatively fast and also provides results with a fair level of accuracy.

Hence, after several attempts, a new mesh arrangement of 189-Hyb with a zonal improvement just before the mouth location was generated that could accurately follow the result of the models with 3.7M and 4.5M cells (Figure 6). This optimal mesh, 189k-HYBcase, had minimum and maximum cell sizes of 0.06 and 0.2 m, respectively, while its surface growth rate was 2.0. This resulted in a dense mesh within 0.8 m from the mouth at the central part of the domain. Table 5 summarizes the applied boundary conditions for the validation test.

***Table 5**. The boundary conditions of the validation case.*

Boundary Type	Boundary Condition	Boundary Value	Air Density	Air Dynamic Viscosity
Inlet	Velocity inlet	20 $m.s^{-1}$	1.184	1.855×10^{-5}
Outlet	Outlet pressure	1 bar	$kg.m^{-3}$	Pa.s
Walls	No-slip	-	-	

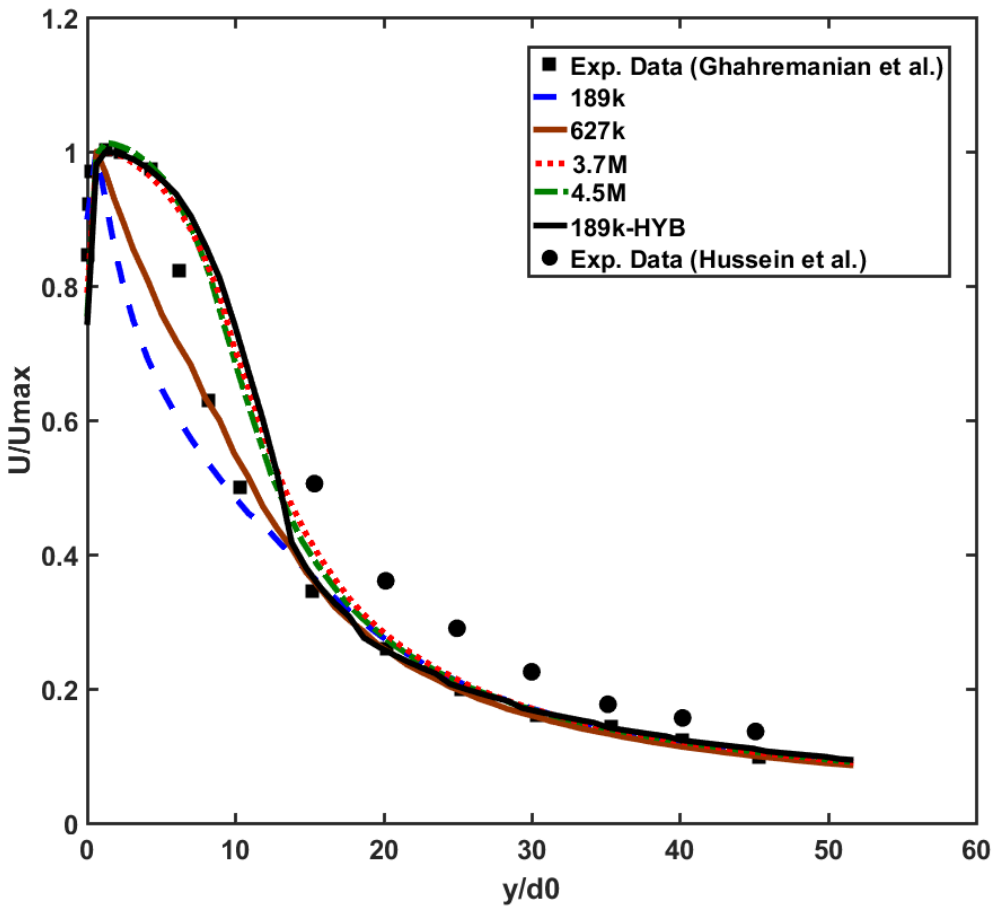

***Figure 5**. Centreline velocity of CFD model compared to the experimental results by (39, 47)*

4.2. Validation of Eulerian CFD Model

The first step in the framework of **Figure 2** is to validate the CFD model. For this purpose, an experimental study by (39) was used for the validation process due to its resemblance to the CFD model. Due to the lack of reliable experimental data on buoyant air jets in the literature, the validation case used in this research work represents an isothermal non-buoyant jet which helped validating the numerical setup applied to the continuum phase (air). The isothermal free turbulent jet experiment provides the spanwise and streamwise velocity profiles at its inlet location with a maximum value of 8.3 m/s. As expected, the Eulerian CFD model of the background flow is in a fair agreement with the experimental results reported by (39) as demonstrated in **Figure 5** while the air velocity at the centerline from the nozzle entrance (y=0) up to the downstream distance of

y=$50d_0$ is compared. Since the risk assessment model is more informative in far distances from the bio-source, it can be concluded that for such distances from the jet source $(y/d_0) > 10$, the results are in general in a better agreement when are compared to the experimental data. As mentioned before, poor predictions of 189k and 672k meshes at $(y/d_0) < 10$ regions, was successfully resolved using a coarse mesh, but carefully adjusted size at different regions of the domain (189-HYB). As a result, the maximum error observed at $(y/d_0) > 10$ region increases from 7% to 10% as it is switched from 4.5M cell mesh to 189-HYB. Thus, this mesh size considerably reduces CPU time from order of months to order of weeks where performing numerous numerical simulations were needed. The validation study with more details using multiple metrics can be found in (34).

Another similar set of experimental data reported by (47) is depicted in **Figure 5** to better evaluate the numerical simulation. It should be noted that the maximum velocity of the recently mentioned research work is 56.2 m/s. Although numerical simulations show a higher deviation compared with experimental data of (47), the trend is still satisfactory with a smaller decrease in the downstream $((y/d_0) > 30)$.

4.3. RAM model

The third step of the proposed framework is investigated in this section. As introduced in **Table 4**, 35 scenarios were simulated in this study, covering wide range of respiratory droplet release events. As explained earlier, the RAM model (34) syntheses the CFD output data to generate an accumulative temporal status of droplets in front of a bio-source. The model counts droplets of any size at any location around the bio-source within the simulation time frame and marks that as a risky location when the number exceeds a defined critical threshold. Here, this value is defined as 100 following a study by (48). Nonetheless, the model can be promptly adjusted to any other suggested numbers.

RAM is an effective tool to monitor the risk cloud expansion through time in a specific environmental and background flow condition. As seen in a base case of **Figure 6a**, the vertical and horizontal spread of risk cloud are separately illustrated after one minute of droplets' release of cough while the tendency of the risk cloud expansion is toward the ceiling. While the relative humidity of 20% is an extreme condition in a typical room temperature of 22℃, such information is handy to decide on the environmental control, HVAC design, and social distancing standards. This implies any person who stays one minute in the 1.0m vicinity of the bio-source can be subject

to the infection. As shown in the following figure, time is a key in the airborne pathogen transmission, and while it is well understood, it is neglected in many risk-assessment studies.

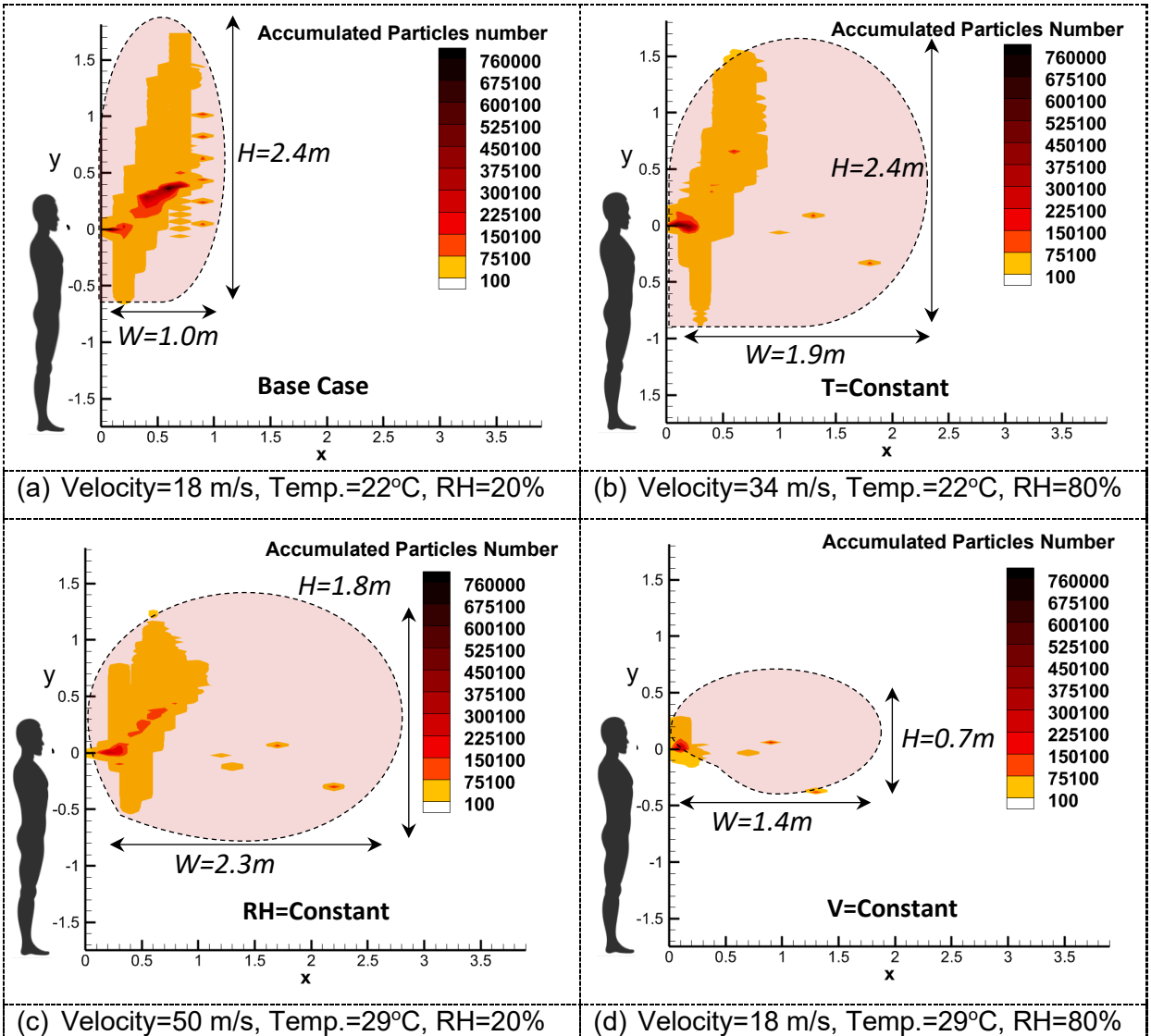

(a) Velocity=18 m/s, Temp.=22°C, RH=20%

(b) Velocity=34 m/s, Temp.=22°C, RH=80%

(c) Velocity=50 m/s, Temp.=29°C, RH=20%

(d) Velocity=18 m/s, Temp.=29°C, RH=80%

Figure 6. RAM model performance for a wide range of parameter variations; (a) Case 4, (b) Case 15, (c) Case 25, and (d) Case 9 after 60 seconds

When two out of three of the selected parameters are varied, as depicted in **Figure 6b to Figure 6d**, the risk cloud can drastically change. An example is **Figure 6b,** where a sneeze event is shown in an RH of 80%. Once again, a person should not stay in a 1.9m vicinity of an infected bio-source for one minute and more. As shown in Figure 7c, a sneeze in a hot and dry climate can even cause a stronger risk cloud horizontally and vertically. Inversely, as initially suggested by many studies (49, 50), a humid climate (e.g., RH>60%) can yet be a safer environment in terms of disease transmission via airborne means. This marginal pattern of risk cloud expansion

can be seen in **Figure 6d,** consistent with the former studies. The following sections will present the time evolution of these clouds in more detail.

In order to demonstrate the effects of ambient relative humidity on the variations of the plume and the movement of the droplets, the velocity fields and particle dispersions of cases 4 and 15 are shown in **Error! Reference source not found.**. Both cases have identical temperature, while the relative humidity and the sneeze velocity are different. As it can be seen, the locations of the fallen heavier droplets depend on the sneeze velocity (the initial velocity of the particles). However, since the locations of the airborne droplets are relatively the same, one can conclude that that the transmission of these droplets is mainly affected by the relative humidity rather than the initial velocity. This finding can be explained by considering the fact that small droplets lose their initial momentum because of the drag force, and then cannot travel much dissimilar from each other as the large droplets can. Since the initial sneeze velocity for these two cases are different, the small airborne droplets will follow different velocity fields created by two sneezes, leading to two different droplet dispersions.

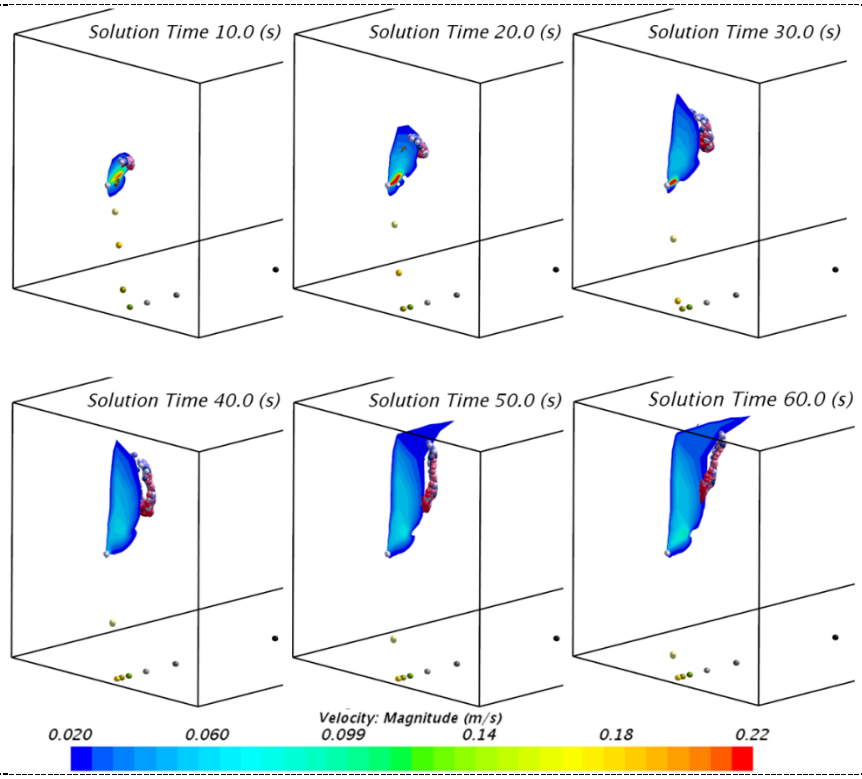

(a)

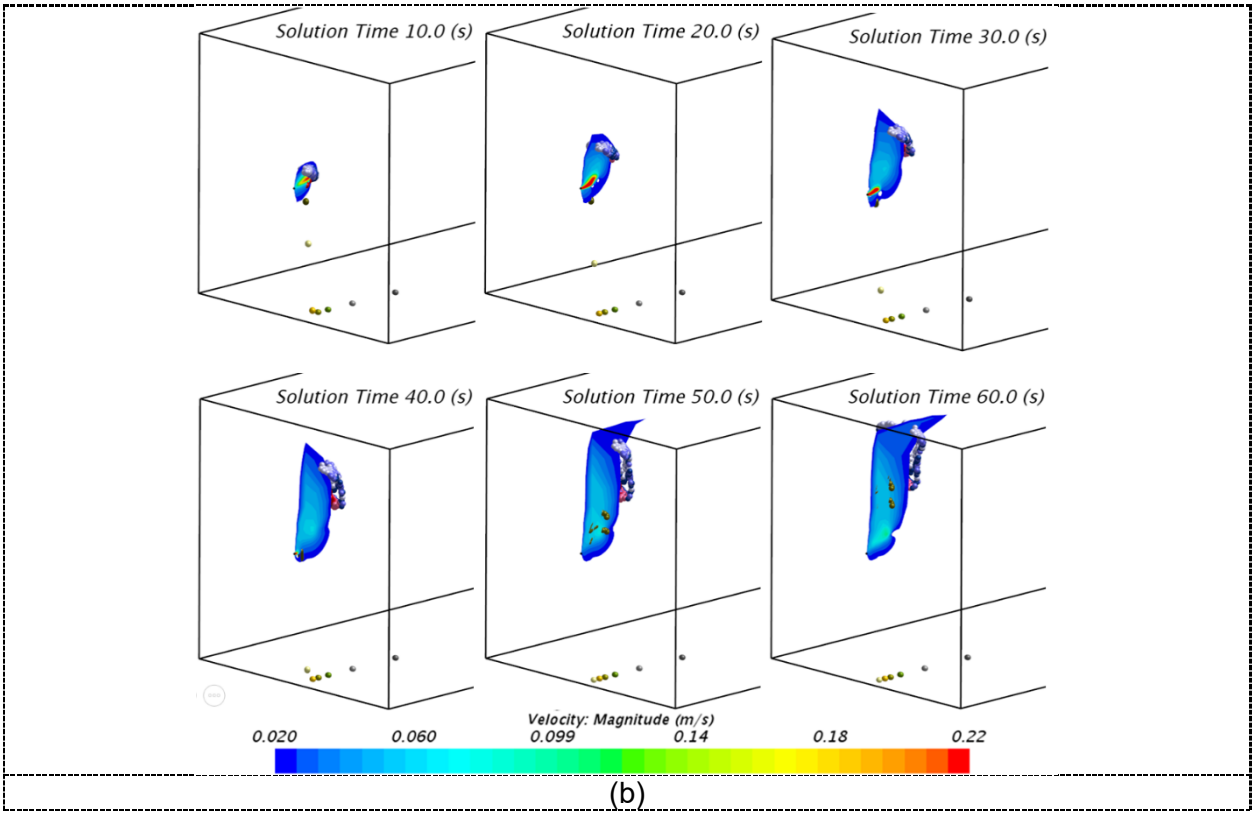

(b)

Figure 7.Time-dependent behaviour of exhaled droplet and the background flow contour for cases (a) Velocity=18 m/s, Temp.=22℃, RH=20% and (b) Velocity=34 m/s, Temp.=22℃, RH=80%

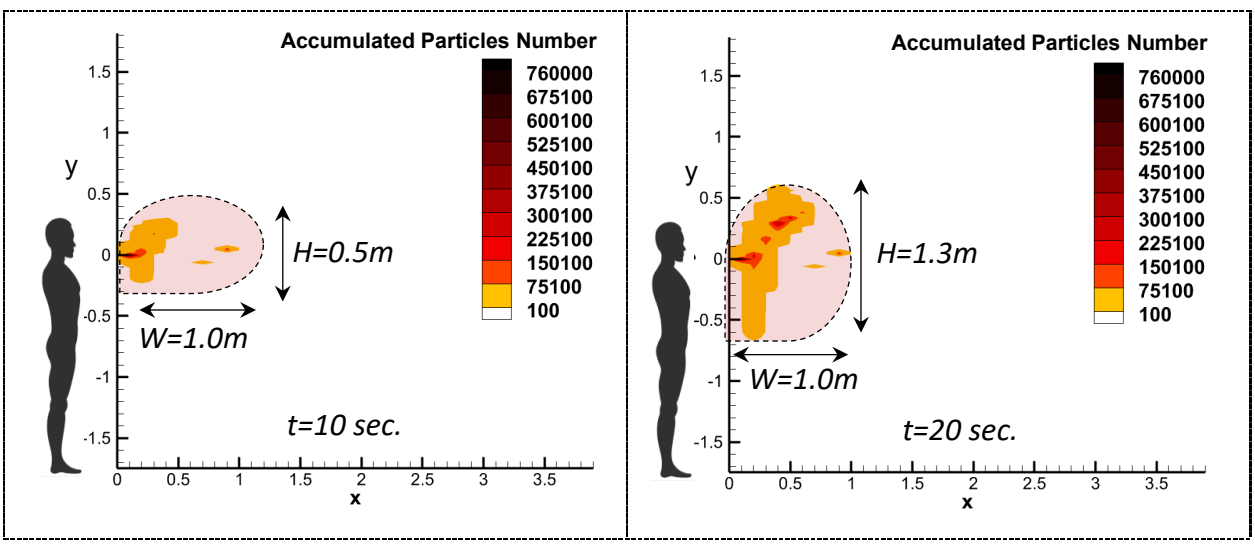

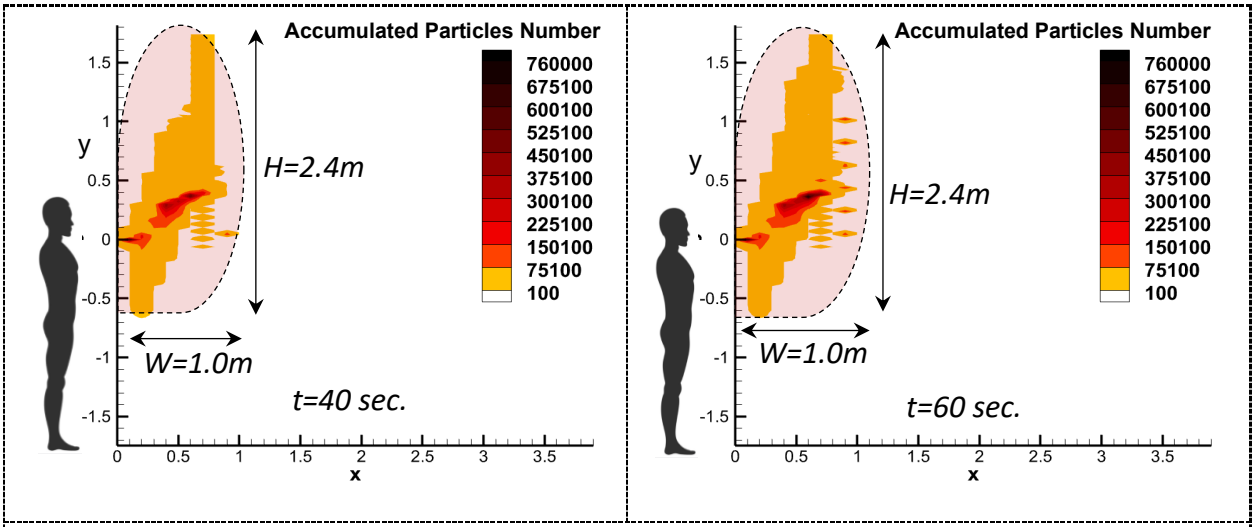

Figure 8. Temporal performance of RAM model for Case 4(Velocity=18 m/s, Temp.=22°C, and RH=20%)

As shown in **Figure 8**, a cough case study with a typical room temperature of 22℃ and low RH of 20% is again demonstrated for time snapshots of 10s, 20s, 50s, and 60s. While the risk cloud reaches 1.0m only in few seconds, it is mainly vertically expanded from few centimeters to about the ceiling height. For this specific case, and as an example where extractors are ceiling mounted, RAM can help to attain similar environmental conditions in this room. Inversely, **Figure 9** shows a sneeze case (Case 27) with a temperature of 29℃ and a low RH of 80%, where the risk cloud is quickly expanded toward the ground and almost remains temporally the same. Therefore, if a room has a ventilation system with a floor-mounted extractor, controlling the environmental condition toward achieving the same risk cloud expansion can be a better solution while enacting a 2.4m distance rule between occupants.

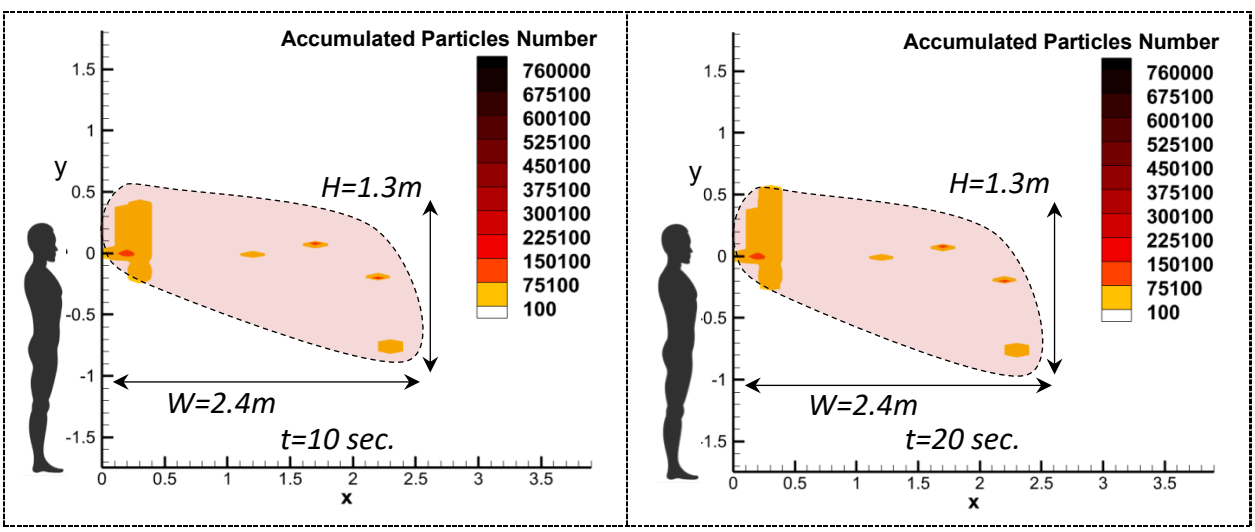

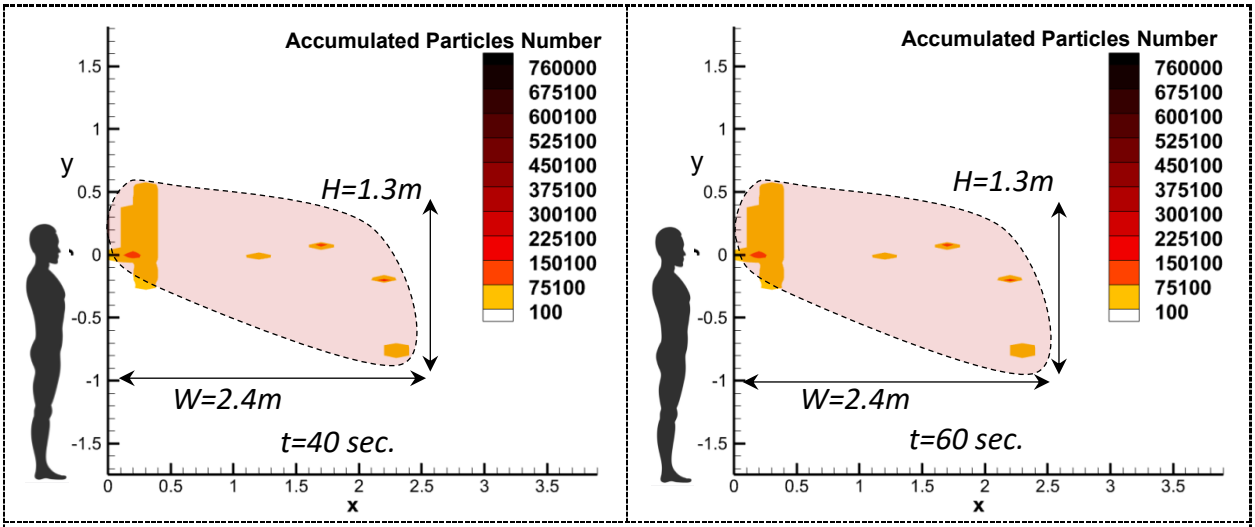

Figure 9. Temporal performance of RAM model for Case 27 (Velocity=50 m/s, Temp.=29°C, and RH=80%)

4.4. Predictive Model

The synthesized vertical and horizontal spread of RAM profiles of data cases in **Table 4** is depicted in **Figure 10**. As stated before, thirty-five training cases are simulated with the CFD model in addition to two testing cases.

Regarding the horizontal spread of the exhaled droplets for these 35 different conditions, as depicted in **Figure 10a**, many of the curves are overlapped and cannot be distinguished from each other. Consequently, until t=30 s, all cases can be classified into six groups in which no horizontal progress can be observed. It should be mentioned that in the horizontal risk measurement, the distance between two successive horizontal planes is 0.1 m. From the beginning of the numerical experiment (t=1s), the horizontal spread of droplets starts at minimum values of 1m for V=18 m/s. As the exhalation velocity increases, the initial horizontal spread also increases such that for V=50 m/s, the horizontal spread at the initial time step reached 1.8 m/s. In most cases, no evolution of the risk cloud on the horizontal spread is detected, mainly because of the particle dynamics due to drag and buoyant forces that progressively become significant in the vertical direction and change droplets to upward direction.

Regarding to the vertical expansion as illustrated in **Figure 10b**, three main regimes can be identified in the data as highlighted in the graph. Regime I is associated with a sudden vertical expansion of the risk cloud (below 30s) when small droplets are affected by the buoyant plume of the exhaled jet. It should be noted that depicted lines represent the vertical spread of droplets, which does not necessarily reflect the air stream pathways. The upward motion of droplets is

caused by the lifting up carrier phase and buoyancy, which is caused by the temperature difference between the exhaled flow and room temperature. An example is a cold and dry climate of Case 19 (temperature of 15℃ and RH of 20%), where the jet plume is expected to push many of the droplets upward, undergoing quick evaporations while being broken to smaller droplets.

Nonetheless, it should be mentioned that it is not a straightforward procedure to draw a general conclusion on the expansion pattern of cloud risk. This further justifies the necessity of developing models similar to RAM to predict safe distances in complex environmental conditions. Regime II is a more frequent pattern for the risk cloud movement as droplets tend to gradually elevate toward the ceiling. The pattern is again very complex to be generalized. Eventually, Regime III states those few cases mainly with a temperature of 29℃ and RH of 80% (e.g., 9, 18, 27). The rate of evaporation in these cases is very low, and the plume is not very strong due to a lower temperature difference between jet and room. Hence, a horizontal spread of the risk cloud can be seen in **Figure 10a**.

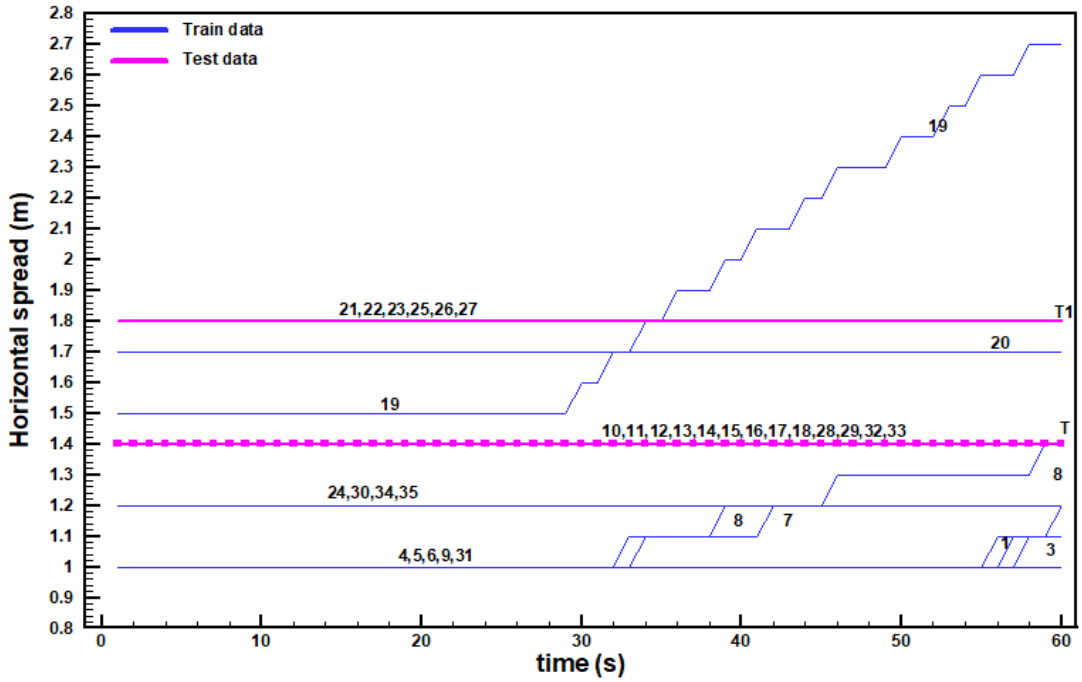

(a)

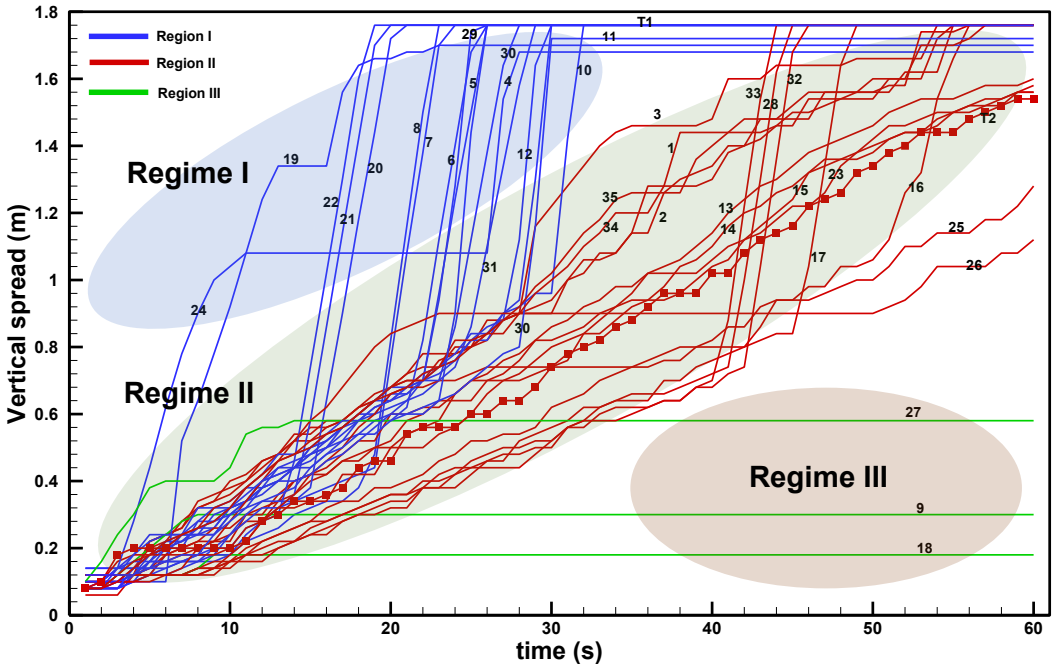

(b)

Figure 10. Synthesized (a) vertical and (b) horizontal spread of RAM profiles of data cases of **Table 4**

Eventually, two samples from Regimes I and II are selected to show the performance of the training process after 1M iterations using the backpropagation method. Regime III was omitted as its behavior is clearer to be predicted without using a complex predictive model. As mentioned before, the ANN inputs are velocity, temperature, humidity, and time where the output of the ANN is spread of droplets in the vertical or horizontal direction. Also, the criteria to stop the training iteration of ANN was the discrepancy of the predicted value with respect to the CFD value to reach below a small value, namely 0.001. Moreover, it should be mentioned that the below-chosen test cases are considered extreme prediction cases in which ANN did not priory include any of the temporal vertical spread evolution.

As seen in **Figure 11a**, the expected values are plotted against ANN output predicted values in addition to lines of ±10% error. **Figure 11b** shows the transient evolution of the vertical risk cloud predicted by the ANN model. The averaged relative error of all test cases calculated by averaging 60 data samples in each training case is about 9.2% (i.e., 2,100 training data samples), which can be considered a fair relative error over the used datasets. Some cases in regime I demonstrate higher relative errors (e.g., Case 24 with 14.2% error) due to the sudden change in the data pattern as the role of both buoyant and drag forces are simultaneously significant and challenging to be projected.

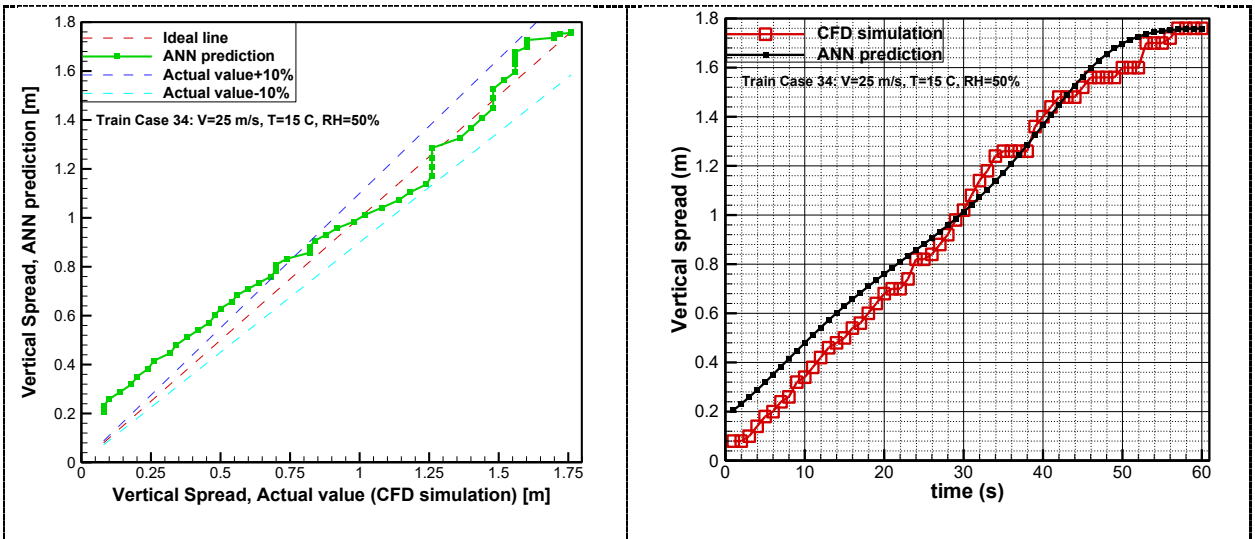

(a) (b)

Figure 11. (a) Training performance of ANN for actual values versus predicted values, and (b) the comparison of ANN model with the CFD simulation for Case 34 (Velocity=25 m/s, Temp.=15°C, and RH=50%)

Figure 12a shows the performance of ANN in the prediction of Case T1 as it adapts itself with the CFD data through the risk cloud spread in the vertical direction within one minute. The ANN model demonstrates a fair prediction up to 50s. In contrast, after this range, even though the CFD data within the time interval between 50s and 60s shows a monotonically increasing behavior, the ANN predicts nearly constant values at this range. The reason lies within several training cases that have these characteristics in which, in a pretty long period of the last seconds, the vertical spread has a constant maximum value. This long period of constant height for the risk cloud can also be seen in the second test case (Case T2). As seen in Figure 12b, the same issue and even more severe remains for the temporal prediction of Case T2.

Nonetheless, the ANN model can reasonably predict the final vertical expansion of the risk cloud, as it can be seen in and Figure 12b. In both parts of Figure 13, ANN not only could follow the trend, but it could precisely predict the exact value. However, where there is a rapid and sharp gradient, ANN shows a less precision. In general, the ANN performance on the prediction of both validation cases can be considered satisfactory as the average error for the vertical spread prediction of risk cloud is about 29.6%. This implies that the developed model can anticipate the temporal variation of risky distances even though the model underperforms for some intervals. This flaw can be mitigated by increasing the dataset size though the main aim of this paper is to conduct a feasibility study to develop an early model to simply estimate the temporal risk cloud expansion.

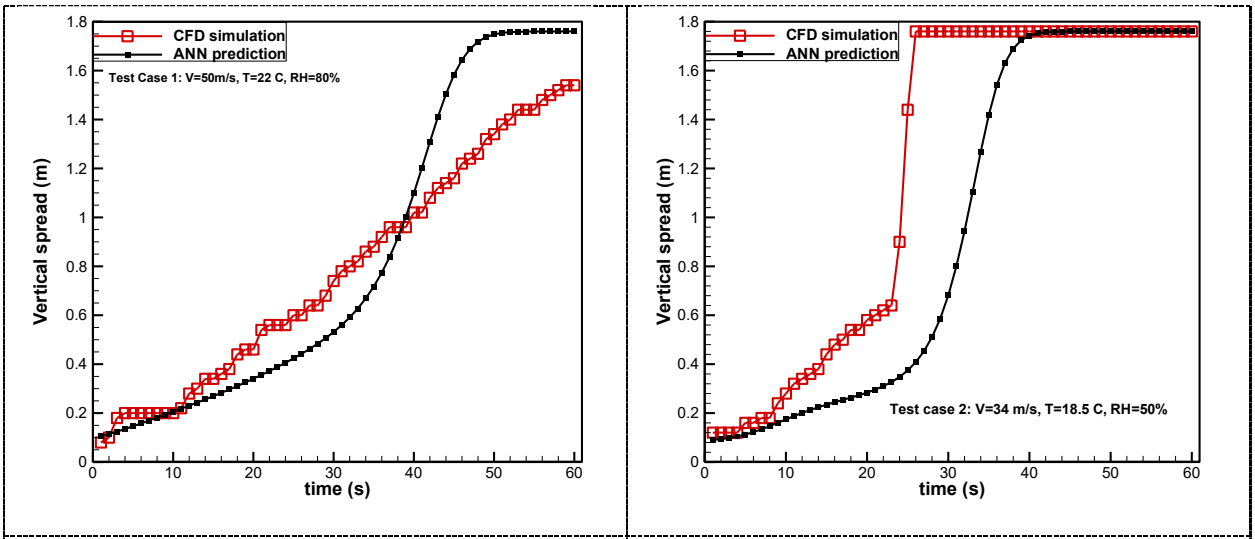

(a) (b)

Figure 12. ANN performance in prediction of (a) Case T1 and (b) Case T2

The step-by-step growing of the training cases' population and its effect on the averaged ANN training error is depicted in Table 6. For each step when the number of cases is increased, it is possible to evaluate the ANN training error. As the population of the training cases grows, the overall performance of the employed ANN increases while there is a decrease in the average and maximum values of the relative error for all cases.

Table 6. *ANN relative error for different number of training cases.*

Number of Training Cases	Averaged Relative Error	Maximum Relative Error
5	27.9 %	59.4%
15	18.3 %	45.8%
25	13.7 %	31.5%
35	9.2 %	26.7%

5. Conclusion

Safe distance against airborne pathogen transmission is a parameter of space and the exposure time to various sizes of virus-laden droplets released from a bio-source. This paper proposes a framework to develop a surrogate model to be assigned to bio-sources instead of running intensive CFD simulations, to predict risk clouds released from them. Thus, a CFD model is first developed to simulate a range of parameters, covering many aspects of respiratory events, including clinical factors such as droplet release velocity, number and distribution of droplets, evaporation of droplets, and environmental factors, including room temperature and humidity. Then, 35 case studies have been defined and simulated to generate a comprehensive dataset. The CFD results have been analyzed based on a tempo-spatial-based risk assessment model (35) previously developed by the authors, which determines the vertical and horizontal spread of respiratory droplets. The surrogate model based on an artificial neural network is then fitted to data to successfully predict the size of the risk cloud around a bio-source under different climatic and clinical conditions.

According to the simulated cases, the vertical spread of droplets can be divided into three regimes with different trends. Some cases are under strong impact of plume while others are mildly or not influenced. This is beneficial since it is an indication of generalization in the behavior of the exhaled jets. Thus, it is expected that the trained ANN to also reflect such generalization in its predictions. Consequently, as the thermal plumes and ventilation systems are not considered in this study, these parameters are among the limitations of this research.

Moreover, thet results suggest that it is possible to apply ANN to a series of simplified CFD cases to generate a simplified calculation model for estimating safe social distances and ventilation designs under different environmental situations, which is more practical for non-experts to use.

Although the predicted results calculated by ANN are satisfactory for the test cases, successful implementation of the ANN tool to real cases needs more comprehensive CFD models that include background airflow, movement of subjects, a higher number of case studies, and also precise clinical data on the infective dosages. Hence, this study is an early step toward developing simplified models, and the developed CFD and RAM models can be subject to continuous improvements from the viewpoint of accuracy.

Future works should include other parameters such as background airflow impacted by occupants and ventilation means (mechanical and natural). Also, more simulations can be undertaken to enhance the performance of the predictive model. Eventually, more clinical data shall be collected to enhance the quality of the CFD model.

Acknowledgment

The faculty of Engineering of The University of Nottingham is acknowledged. Academy of Finland under grant no. 314487 is acknowledged. The author would like to acknowledge the computational support of Sogang University Research Grant of 2019 (201919069.01).

References

1. Cevik M, Kuppalli K, Kindrachuk J, Peiris M. Virology, transmission, and pathogenesis of SARS-CoV-2. BMJ. 2020;371:m3862.
2. Jones NR, Qureshi ZU, Temple RJ, Larwood JPJ, Greenhalgh T, Bourouiba L. Two metres or one: what is the evidence for physical distancing in covid-19? BMJ. 2020;370:m3223.
3. Mittal R, Ni R, Seo J-H. The flow physics of COVID-19. Journal of Fluid Mechanics. 2020;894:F2.
4. Lindsley WG, Reynolds JS, Szalajda JV, Noti JD, Beezhold DH. A Cough Aerosol Simulator for the Study of Disease Transmission by Human Cough-Generated Aerosols. Aerosol Science and Technology. 2013;47(8):937-44.
5. Vuorinen V, Aarnio M, Alava M, Alopaeus V, Atanasova N, Auvinen M, et al. Modelling aerosol transport and virus exposure with numerical simulations in relation to SARS-CoV-2 transmission by inhalation indoors. Safety Science. 2020;130:104866.
6. Aliabadi A, Rogak S, Green S, Bartlett K, editors. CFD Simulation of Human Coughs and Sneezes: A Study in Droplet Dispersion, Heat, and Mass Transfer2010.
7. Stabile L, Arpino F, Buonanno G, Russi A, Frattolillo A. A simplified benchmark of ultrafine particle dispersion in idealized urban street canyons: A wind tunnel study. Building and Environment. 2015;93:186-98.
8. Zhang Y, Feng G, Bi Y, Cai Y, Zhang Z, Cao G. Distribution of droplet aerosols generated by mouth coughing and nose breathing in an air-conditioned room. Sustainable Cities and Society. 2019;51:101721.
9. Buonanno G, Lall AA, Stabile L. Temporal size distribution and concentration of particles near a major highway. Atmospheric Environment. 2009;43(5):1100-5.

10. Ren S, Li W, Wang L, Shi Y, Cai M, Hao L, et al. Numerical Analysis of Airway Mucus Clearance Effectiveness Using Assisted Coughing Techniques. Scientific Reports. 2020;10(1):2030.
11. Tang JW, Liebner TJ, Craven BA, Settles GS. A schlieren optical study of the human cough with and without wearing masks for aerosol infection control. Journal of The Royal Society Interface. 2009;6(suppl_6):S727-S36.
12. Kwon S-B, Park J, Jang J, Cho Y, Park D-S, Kim C, et al. Study on the initial velocity distribution of exhaled air from coughing and speaking. Chemosphere. 2012;87(11):1260-4.
13. Villafruela JM, Olmedo I, Ruiz de Adana M, Méndez C, Nielsen PV. CFD analysis of the human exhalation flow using different boundary conditions and ventilation strategies. Building and Environment. 2013;62:191-200.
14. Ren S, Niu J, Luo Z, Shi Y, Cai M, Luo Z, et al. Cough Expired Volume and Cough Peak Flow Rate Estimation Based on GA-BP Method. Complexity. 2020;2020:9036369.
15. Zayas G, Chiang MC, Wong E, MacDonald F, Lange CF, Senthilselvan A, et al. Cough aerosol in healthy participants: fundamental knowledge to optimize droplet-spread infectious respiratory disease management. BMC Pulmonary Medicine. 2012;12(1):11.
16. Galbadage T, Peterson BM, Gunasekera RS. Does COVID-19 Spread Through Droplets Alone? Frontiers in Public Health. 2020;8(163).
17. Wei J, Li Y. Enhanced spread of expiratory droplets by turbulence in a cough jet. Building and Environment. 2015;93:86-96.
18. Anand S, Mayya YS. Size distribution of virus laden droplets from expiratory ejecta of infected subjects. Scientific Reports. 2020;10(1):21174.
19. Hoque S, Omar FB. Coupling Computational Fluid Dynamics Simulations and Statistical Moments for Designing Healthy Indoor Spaces. International Journal of Environmental Research and Public Health. 2019;16(5):800.
20. (Osha) OSaHA. Guidance on Preparing Workplaces for COVID-19. 2020.
21. Stadnytskyi V, Bax CE, Bax A, Anfinrud P. The airborne lifetime of small speech droplets and their potential importance in SARS-CoV-2 transmission. Proceedings of the National Academy of Sciences. 2020;117(22):11875-7.
22. Verma S, Dhanak M, Frankenfield J. Visualizing the effectiveness of face masks in obstructing respiratory jets. Physics of Fluids. 2020;32(6):061708.
23. Berlanga FA, Liu L, Nielsen PV, Jensen RL, Costa A, Olmedo I, et al. Influence of the geometry of the airways on the characterization of exhalation flows. Comparison between two different airway complexity levels performing two different breathing functions. Sustainable Cities and Society. 2020;53:101874.
24. Shih YC, Chiu CC, Wang O. Dynamic airflow simulation within an isolation room. Build Environ. 2007;42(9):3194-209.
25. Wang J, Chow T-T. Numerical investigation of influence of human walking on dispersion and deposition of expiratory droplets in airborne infection isolation room. Building and Environment. 2011;46(10):1993-2002.
26. Gao N, Niu J. Transient CFD simulation of the respiration process and inter-person exposure assessment. Building and environment. 2006;41(9):1214-22.
27. Redrow J, Mao S, Celik I, Posada JA, Feng Z-g. Modeling the evaporation and dispersion of airborne sputum droplets expelled from a human cough. Building and Environment. 2011;46(10):2042-51.
28. Ge Q, Li X, Inthavong K, Tu J. Numerical study of the effects of human body heat on particle transport and inhalation in indoor environment. Building and Environment. 2013;59:1-9.
29. Bourouiba L, Dehandschoewercker E, Bush John WM. Violent expiratory events: on coughing and sneezing. Journal of Fluid Mechanics. 2014;745:537-63.

30. Villafruela JM, Olmedo I, San José JF. Influence of human breathing modes on airborne cross infection risk. Building and Environment. 2016;106:340-51.
31. Zhou Y, Ji S. Experimental and numerical study on the transport of droplet aerosols generated by occupants in a fever clinic. Building and Environment. 2021;187:107402.
32. Cheng CH, Chow CL, Chow WK. Trajectories of large respiratory droplets in indoor environment: A simplified approach. Building and Environment. 2020;183:107196.
33. Yan Y, Li X, Yang L, Yan P, Tu J. Evaluation of cough-jet effects on the transport characteristics of respiratory-induced contaminants in airline passengers' local environments. Building and Environment. 2020;183:107206.
34. Mirzaei; PA, Moshfeghi; M, Motamedi; H, Sheikhnejad; Y, Bordbar; H. A simplified model to estimate COVID19 transport in enclosed spaces. IBPC; Denmark2021.
35. Motamedi Zoka H, Moshfeghi M, Bordbar H, Mirzaei PA, Sheikhnejad Y. A CFD Approach for Risk Assessment Based on Airborne Pathogen Transmission. Atmosphere. 2021;12(8):986.
36. Issues Affecting Respirator Selection for Workers Exposed to Infectious Aerosols: Emphasis on Healthcare Settings. Applied Biosafety. 2004;9(1):20-36.
37. Li X, Shang Y, Yan Y, Yang L, Tu J. Modelling of evaporation of cough droplets in inhomogeneous humidity fields using the multi-component Eulerian-Lagrangian approach. Building and Environment. 2018;128:68-76.
38. Yan Y, Li X, Tu J. Thermal effect of human body on cough droplets evaporation and dispersion in an enclosed space. Building and Environment. 2019;148:96-106.
39. Ghahremanian S, Moshfegh B. Numerical and experimental verification of initial, transitional and turbulent regions of free turbulent round jet. 20th AIAA Computational Fluid Dynamics Conference.
40. Menter FR. Two-equation eddy-viscosity turbulence models for engineering applications. AIAA Journal. 1994;32(8):1598-605.
41. Peng S, Chen Q, Liu E. The role of computational fluid dynamics tools on investigation of pathogen transmission: Prevention and control. Science of The Total Environment. 2020;746:142090.
42. Božič A, Kanduč M. Relative humidity in droplet and airborne transmission of disease. Journal of Biological Physics. 2021;47(1):1-29.
43. Busco G, Yang SR, Seo J, Hassan YA. Sneezing and asymptomatic virus transmission. Physics of fluids (Woodbury, NY : 1994). 2020;32(7):073309-.
44. Chao CYH, Wan MP, Morawska L, Johnson GR, Ristovski ZD, Hargreaves M, et al. Characterization of expiration air jets and droplet size distributions immediately at the mouth opening. Journal of aerosol science. 2009;40(2):122-33.
45. Han ZY, Weng WG, Huang QY. Characterizations of particle size distribution of the droplets exhaled by sneeze. Journal of The Royal Society Interface. 2013;10(88):20130560.
46. Schmidhuber J. Deep learning in neural networks: An overview. Neural Networks. 2015;61:85-117.
47. Hussein HJ, Capp SP, George WK. Velocity measurements in a high-Reynolds-number, momentum-conserving, axisymmetric, turbulent jet. Journal of Fluid Mechanics. 1994;258:31-75.
48. Karimzadeh S, Bhopal R, Nguyen Tien H. Review of infective dose, routes of transmission and outcome of COVID-19 caused by the SARS-COV-2: comparison with other respiratory viruses. Epidemiology and Infection. 2021;149:e96.
49. Morris DH, Yinda KC, Gamble A, Rossine FW, Huang Q, Bushmaker T, et al. Mechanistic theory predicts the effects of temperature and humidity on inactivation of SARS-CoV-2 and other enveloped viruses. bioRxiv. 2020:2020.10.16.341883.
50. Ahlawat A, Wiedensohler A, Mishra SK. An Overview on the Role of Relative Humidity in Airborne Transmission of SARS-CoV-2 in Indoor Environments. Aerosol and Air Quality Research. 2020;20(9):1856-61.

1